10-20-2015

Few-Boson Processes in the Presence of an Attractive Impurity Under One-Dimensional Confinement

Nirav P. Mehta
Trinity University, nmehta@trinity.edu

Connor D. Morehead
Trinity University, cmorehea@trinity.edu

Few-boson processes in the presence of an attractive impurity under one-dimensional confinement

N. P. Mehta* and Connor D. Morehead
Trinity University, San Antonio, Texas 78212-7200, USA
(Received 1 August 2015; published 20 October 2015)

We consider a few-boson system confined to one dimension with a single distinguishable particle of lesser mass. All particle interactions are modeled with δ functions, but due to the mass imbalance the problem is nonintegrable. Universal few-body binding energies, atom-dimer and atom-trimer scattering lengths, are all calculated in terms of two parameters, namely the mass ratio $m_{\rm L}/m_{\rm H}$, and ratio $g_{\rm HH}/g_{\rm HL}$ of the δ-function couplings. We specifically identify the values of these ratios for which the atom-dimer or atom-trimer scattering lengths vanish or diverge. We identify regions in this parameter space in which various few-body inelastic processes become energetically allowed. In the Tonks-Girardeau limit ($g_{\rm HH} \to \infty$), our results are relevant to experiments involving trapped fermions with an impurity atom.

DOI: 10.1103/PhysRevA.92.043616 PACS number(s): 67.85.−d

I. INTRODUCTION

Strongly interacting one-dimensional (1D) quantum systems have been of fundamental interest for many years [1,2]. Not long ago, a number of experiments [3–5] involving quantum gases tightly confined to two-dimensional (2D) optical lattices realized the 1D Lieb-Liniger-McGuire model [6–8]. Interpretation of these experiments in terms of the one-dimensional model parameters has been facilitated by a calculation of the effective 1D coupling constant ($g_{\rm 1D}$) and dimer energy (E_2) in terms of the three-dimensional (3D) s-wave scattering length ($a_{\rm 3D}$) and the transverse confinement length [$a_\perp = (\mu\omega_\perp)^{-1/2}$] [9,10] (in units with $\hbar = 1$ throughout):

$$g_{\rm 1D} = \frac{2a_{\rm 3D}}{\mu a_\perp^2\left(1 - \left|\zeta\left(\frac{1}{2}\right)\right|\frac{a_{\rm 3D}}{a_\perp}\right)}, \quad \zeta\left(\frac{1}{2},\Omega_B\right) = -\frac{a_\perp}{a_{\rm 3D}}, \qquad (1)$$

where $\zeta(z,q)$ is the generalized Riemann ζ function [11], μ is the two-body reduced mass, and $\Omega_B = 1/2 - E_2/(2\omega_\perp)$ is the dimensionless dimer binding energy. The result predicts the so-called "confinement induced resonance" (CIR) when $|\zeta(1/2)|a_{\rm 3D} = a_\perp$, where $|g_{\rm 1D}| \to \infty$ and the 1D scattering length $a_{\rm 1D} = -(\mu g_{\rm 1D})^{-1}$ passes through zero. Remarkably, $g_{\rm 1D}$ can be experimentally tuned by varying either $a_{\rm 3D}$ (via a magnetic Feshbach resonance) or $a_\perp$.

Moreover, Eq. (1) predicts that a 1D dimer always exists below the asymptotic threshold energy $\omega_\perp$ regardless of the sign of $a_{\rm 3D}$. Such confinement-induced dimers have been seen in Monte Carlo simulations [12,13] and observed experimentally by rf spectroscopy [14]. When the axial extent of the dimer is large compared to the transverse confinement length, the few-body physics is expected to follow from a purely 1D calculation with δ-function couplings given by Eq. (1) [12,13,15,16]. This limit is achieved when $a_\perp/a_{\rm 3D} \to -\infty$, such that $\Omega_B \ll 1$.

More recent quasi-1D experiments have begun to probe the interaction of a degenerate quantum gas with a distinguishable impurity [14,17–19]. Motivated by the aforementioned evidence that—in the appropriate limit—purely 1D calculations of few-body processes can provide physically meaningful insights into quasi-1D experiments, we consider here the $N = 3$ and $N = 4$ instances of the following Hamiltonian:

$$H = -\frac{1}{2m_{\rm H}}\sum_{i=1}^{N-1}\frac{\partial^2}{\partial x_i^2} - \frac{1}{2m_{\rm L}}\frac{\partial^2}{\partial x_N^2} + \sum_{i<j}^{N-1} g_{\rm HH}\delta(x_i - x_j) + \sum_{i=1}^{N-1} g_{\rm HL}\delta(x_i - x_N), \qquad (2)$$

where particles 1 through $(N-1)$ are identical bosons (H) of mass $m_{\rm H}$, and particle N is an impurity (L) of mass $m_{\rm L}$. The equal-mass ($m_{\rm L} = m_{\rm H}$) instance of Eq. (2) has been realized with ^{40}K atoms [14] and more recently ^{6}Li [17], with related theory work found in Refs. [20–27]. Note that the Bose-Fermi mapping [28] allows one to consider the $g_{\rm HH} \to \infty$ instance of Eq. (2) for a description of a noninteracting background gas of fermions. The unequal mass case ($m_{\rm H} > m_{\rm L}$) of Eq. (2) has been realized with a ^{41}K impurity in a background gas of ^{87}Rb [18].

We assume that the impurity is of lesser mass than the background atoms, and employ the Born-Oppenheimer method to obtain adiabatic potentials for the heavy-particle motion. In the thermodynamic limit, stability of the background gas requires $g_{\rm HH} > 0$. At the few-body level, our calculation permits us to consider $g_{\rm HH} < 0$, but with the caveat that the lowest scattering threshold involves a bound impurity. The eigenstates of Eq. (2) are completely specified by the coupling ratio $\lambda = g_{\rm HH}/g_{\rm HL}$ and the mass ratio $\beta = m_{\rm L}/m_{\rm H}$. The case $N = 3$ of Eq. (2) has been studied in considerable detail by Kartavtsev *et al.* [29], who treat all possible values of λ and β using the adiabatic hyperspherical representation. Mehta [30] used the Born-Oppenheimer method to extend those results to the case $N = 4$, but only considered the cases $\lambda \to 0$ and $|\lambda| \to \infty$ with $\beta \leqslant 1$. This work is an extension of those calculations to finite values of λ. Some of the approximate $N = 3$ calculations presented here can be directly compared to the benchmark calculations of [29], but we are unaware of similar calculations for $N = 4$.

We calculate the atom-dimer scattering length $a_{\rm AD}$, the atom-trimer scattering length $a_{\rm AT}$, and trimer and tetramer bound-state energies as a function of β and λ. The critical values of β and λ at which these scattering lengths diverge

*nmehta@trinity.edu

are identified and marked by the appearance of a new bound state. We find that few-body bound states tend towards deeper binding as one increases λ (making it less negative) or increases β^{-1}. This behavior allows us to identify the critical values of λ and β where particular inelastic processes become energetically allowed.

II. BORN-OPPENHEIMER SOLUTION

Here we briefly sketch the Born-Oppenheimer calculation. Many elements of the derivation are unchanged from [30], so we present an abridged derivation sufficient to highlight changes due to choosing finite $\lambda = g_{\rm HH}/g_{\rm HL}$.

We scale the Hamiltonian by the HL binding energy $B_2 = \mu_{\rm HL} g_{\rm HL}^2/2 = 1/(2\mu_{\rm HL} a^2)$ and use the HL scattering length $a = -1/(\mu_{\rm HL} g_{\rm HL}) > 0$ as the fundamental length unit. The calculation of few-body observables in a homogeneous system begins the removal of the center-of-mass motion by a transformation to mass-scaled Jacobi coordinates $\{x,y,z\}$:

$$\begin{aligned} x &= \frac{1}{a}\sqrt{\frac{\mu_{12}}{\mu_{4b}}}(x_1 - x_2), \\ y &= \frac{1}{a}\sqrt{\frac{\mu_{12,3}}{\mu_{4b}}}\left(\frac{m_1 x_1 + m_2 x_2}{m_1 + m_2} - x_3\right), \\ z &= \frac{1}{a}\sqrt{\frac{\mu_{123,4}}{\mu_{4b}}}\left(\frac{m_1 x_1 + m_2 x_2 + m_3 x_3}{m_1 + m_2 + m_3} - x_4\right). \end{aligned} \tag{3}$$

Here $\mu_{4b} = (\mu_{12}\mu_{12,3}\mu_{123,4})^{1/3}$ is the four-body reduced mass, and $\mu_{a,b}$ is a two-body reduced mass between clusters a and b. The coordinates for the three-particle problem are the same, but with the z-coordinate omitted and μ_{4b} replaced by $\mu_{3b} = (\mu_{12}\mu_{12,3})^{1/2}$.

A. Three-body problem

The Born-Oppenheimer factorization of the three-body wave function $\Psi(x,y) = \Phi(x;y)\psi(x)$ requires that $\Phi(x;y)$ be an eigenstate of the fixed-x Hamiltonian:

$$H_{ad}^{(3)} = -\frac{1}{2\mu_3}\frac{\partial^2}{\partial x^2} + g_3[\delta(y - x_0) + \delta(y + x_0)], \tag{4}$$

with x-dependent eigenvalue $u(x)$. We have defined the unitless three-body reduced mass $\mu_3 = (1+\beta)/[2\sqrt{\beta(2+\beta)}]$, coupling $g_3 = -2\sqrt{2}[\beta/(2+\beta)]^{1/4}$, and scaled heavy-particle separation $x_0 = x\sqrt{\beta/(2+\beta)}$. The solution to Eq. (4) yields the following transcendental equation for the lowest $u(x)$:

$$\frac{\kappa}{g_3\mu_3} + 1 = -\exp(-2\kappa x_0), \tag{5}$$

where $\kappa = \sqrt{-2\mu_{\rm HL} u(x)}$. The heavy-particle wave function $\psi(x)$ is now governed by the effective Hamiltonian:

$$H_{\rm eff}^{(3)} = \frac{-1}{2\mu_3}\frac{\partial^2}{\partial x^2} + g_3\lambda\delta(2x_0) + u(x) + \frac{\tilde{Q}(x)}{2\mu_3}. \tag{6}$$

Here $\tilde{Q}(x) = \langle\Phi'|\Phi'\rangle_y$ is the diagonal nonadiabatic correction, where the primes denote derivatives with respect to the slow coordinate x, and the integration is carried out over the fast coordinate y only. Ignoring $\tilde{Q}(x)$ leads to a lower bound on the three-body ground-state energy, while including $\tilde{Q}(x)$ leads to an upper bound that is typically more accurate [31–34]. We refer to the former calculation as the "extreme adiabatic approximation" (EAA) and the latter as the "uncoupled adiabatic approximation" (UAA). The cases $\lambda = 0$ and $|\lambda| \to \infty$ were treated in [30]. Here we consider arbitrary λ, and replace the δ function in Eq. (6) with the following boundary condition on the solution $\psi(x)$ for $x > 0$:

$$\left(\frac{1}{\psi}\frac{\partial\psi}{\partial x}\right)_{x\to 0^+} = -\lambda\frac{1+\beta}{\sqrt{2\beta}[\beta(2+\beta)]^{1/4}}. \tag{7}$$

B. Four-body problem

For the four-particle problem, it is convenient to work in "hypercylindrical" coordinates, trading $\{x,y,z\} \to \{\rho,\phi,z\}$ by the usual transformation: $\rho^2 = x^2 + y^2$, and $\tan\phi = y/x$. We make the Born-Oppenheimer factorization: $\Psi(\rho,\phi,z) = \Phi(\rho,\phi;z)\psi(\rho,\phi)$, and integrate out the light-particle degree of freedom by demanding $\Phi(\rho,\phi;z)$ be an eigenstate of the following fixed-$\{\rho,\phi\}$ Hamiltonian with eigenvalue $U(\rho,\phi)$:

$$H_{ad}^{(4)} = \frac{-1}{2\mu_4}\frac{\partial^2}{\partial z^2} + g_4\sum_{i=1}^{3}\delta(z - z_i). \tag{8}$$

We have again introduced unitless parameters: $\mu_4 = (\beta+1)/[2\beta^{2/3}(3+\beta)^{1/3}]$ and $g_4 = -2\sqrt{3}[\beta/(3+\beta)]^{1/3}$. The heavy-light coalescence points occur at $z_i = \sqrt{2\beta/(3+\beta)}\,\rho\sin(\phi - \phi_i)$ with $\phi_1 = -4\pi/3$, $\phi_2 = 0$, and $\phi_3 = -2\pi/3$. The adiabatic equation is simply a triple-δ problem that leads to the following transcendental equation for the potential energy surface:

$$\frac{(g+2\kappa)^2}{g^2}e^{2\kappa z_3} + \frac{(g-2\kappa)}{g+2\kappa}e^{2\kappa z_1} = e^{2\kappa z_2} + e^{2\kappa(z_1 - z_2 + z_3)}, \tag{9}$$

where $g = 2\mu_4 g_4$, $\kappa^2 = -2\mu_4 U(\rho,\phi) > 0$.

The heavy-particle eigenstates $\psi(\rho,\phi)$ now live on the potential energy surface $U(\rho,\phi)$, and are eigenstates of the effective Hamiltonian (in the EAA):

$$\begin{aligned} H_{\rm eff}^{(4)} = &\frac{-1}{2\mu_4}\left(\frac{1}{\rho}\frac{\partial}{\partial\rho}\rho\frac{\partial}{\partial\rho} + \frac{1}{\rho^2}\frac{\partial^2}{\partial\phi^2}\right) \\ &+\left[U(\rho,\phi) + \frac{\lambda g_4}{\alpha\rho}\sum_{i<j}^{3}\delta(|\sin(\phi - \phi_{ij})|)\right], \end{aligned} \tag{10}$$

where $\alpha = \sqrt{6\beta/(3+\beta)}$. In order to extract scattering lengths we require a representation of the wave function that gives the appropriate asymptotic cluster states. We write $\psi(\rho,\phi) = \sum_{n=0}^{\infty}\rho^{-1/2} f_n(\rho)\chi_n(\rho;\phi)$, where the channel functions χ_n satisfy the fixed-ρ equation:

$$\frac{-1}{2\mu_4\rho^2}\frac{\partial^2\chi_n}{\partial\phi^2} + U(\rho,\phi)\chi_n = U_n(\rho)\chi_n. \tag{11}$$

Due to identical particle symmetry, one only needs to consider the restricted range $\phi \in [0,\pi/6)$ with the boundary condition [30]

$$\lim_{\epsilon\to 0}\frac{1}{\chi}\frac{\partial\chi}{\partial\phi}\bigg|_{\pi/6-\epsilon} = \frac{\rho\lambda(1+\beta)}{\sqrt{2\beta}}\left(\frac{\beta}{3+\beta}\right)^{1/6}. \tag{12}$$

TABLE I. The boundary conditions on the channel functions $\chi_n(\rho;\phi)$ for the noninteracting (NI), infinitely repulsive (IR) cases are summarized here.

	(+) parity	(−) parity
NI bosons	$[\frac{\partial\chi}{\partial\phi}]_{\phi=0}=0\,[\frac{\partial\chi}{\partial\phi}]_{\phi=\pi/6}=0$	$\chi\|_{\phi=0}=0\,[\frac{\partial\chi}{\partial\phi}]_{\phi=\pi/6}=0$
IR bosons	$[\frac{\partial\chi}{\partial\phi}]_{\phi=0}=0\,\chi\|_{\phi=\pi/6}=0$	$\chi\|_{\phi=0}=0\,\chi\|_{\phi=\pi/6}=0$
NI fermions	$\chi\|_{\phi=0}=0\,\chi\|_{\phi=\pi/6}=0$	$[\frac{\partial\chi}{\partial\phi}]_{\phi=0}=0\,\chi\|_{\phi=\pi/6}=0$

Finally, the four-particle problem is reduced to a set of coupled equations in ρ only:

$$\frac{-1}{2\mu_4}\left(\mathbf{1}\frac{\partial^2}{\partial\rho^2}+\mathbf{Q}(\rho)+2\mathbf{P}(\rho)\frac{\partial}{\partial\rho}\right)\vec{f}(\rho)+\mathbf{U}_{\rm eff}(\rho)\vec{f}(\rho)=E_{EAA}\vec{f}(\rho). \tag{13}$$

Here $\mathbf{U}_{\rm eff}$ is a diagonal matrix with elements $U_n(\rho)-1/8\mu_4\rho^2$, $P_{mn}(\rho)=\langle\chi_m|\chi_n'\rangle_\phi$, and $Q_{mn}(\rho)=\langle\chi_m|\chi_n''\rangle_\phi$. The Born-Oppenheimer potentials obtained from Eqs. (5) and (9) are independent of λ, and only need to be calculated once for a given β. The λ dependence only appears through the boundary conditions (7) and (12).

In Table I we summarize the boundary conditions on the channel functions $\chi_n(\rho;\phi)$. Note that starting with positive parity noninteracting bosons, one achieves the infinitely repulsive "fermionized" limit as $\lambda\to-\infty$ (since $g_{\rm HL}<0$). Equation (12) then gives a boundary condition identical to that of noninteracting fermions, but of negative parity. Due to Pauli exclusion, identical (spin-polarized) fermions are insensitive to the zero-range interaction, and the boundary conditions for fermions are unaffected by λ.

III. NUMERICAL SOLUTIONS

Born-Oppenheimer and hyper-radial potential curves provide a view of the few-body energy landscape that aids in the interpretation subsequent calculations. In Figs. 1(a) and 1(b) we show potential curves and bound state energies for the Li-Cs mass ratio $\beta^{-1/2}=4.7$, and $\lambda\to-\infty$. Figure 1(a) shows the hyper-radial potential curves $U_n(\rho)$ while Fig. 1(b) shows the effective H-H interaction $u(x)$. Tetramer $(HHHL)$ and trimer (HHL) bound states are indicated by dashed red lines in Figs. 1(a) and 1(b), respectively. Figures 1(c) and 1(d) and Figs. 1(e) and 1(f) are identical to Figs. 1(a) and 1(b), but for $\lambda=-1$ and $\lambda=0$, respectively. Note that the potential curves $U_n(\rho)$ depend on λ through the boundary condition (12). While $u(x)$ is independent of λ, the trimer binding energies depend on λ through Eq. (7).

In the limit $\rho\to\infty$, the lowest potentials $U_n(\rho)$ approach the trimer energies, asymptotically representing atom-trimer channels $(H+HHL)$. In the lowest atom-trimer channel we clearly see the appearance of a short-range potential energy barrier as $\lambda\to-\infty$. This barrier is a direct result of the boundary condition (12), and represents the repulsive effect of fermionization. We also see a set of potentials asymptotically approaching the dimer energy $U_n/B_2=-1$. These represent the three-body $(H+H+HL)$ channels. Three-body recombination at threshold is controlled by the lowest such potential, which in the large ρ limit behaves as $U_n(\rho)\to\kappa_{\rm min}^2/(2\mu_4\rho^2)$. A full hyperspherical calculation would also produce a set of potentials approaching the zero-energy threshold asymptotically representing four free atoms $(H+H+H+L)$. Our calculation cannot capture these potentials because the light particle is required to be bound.

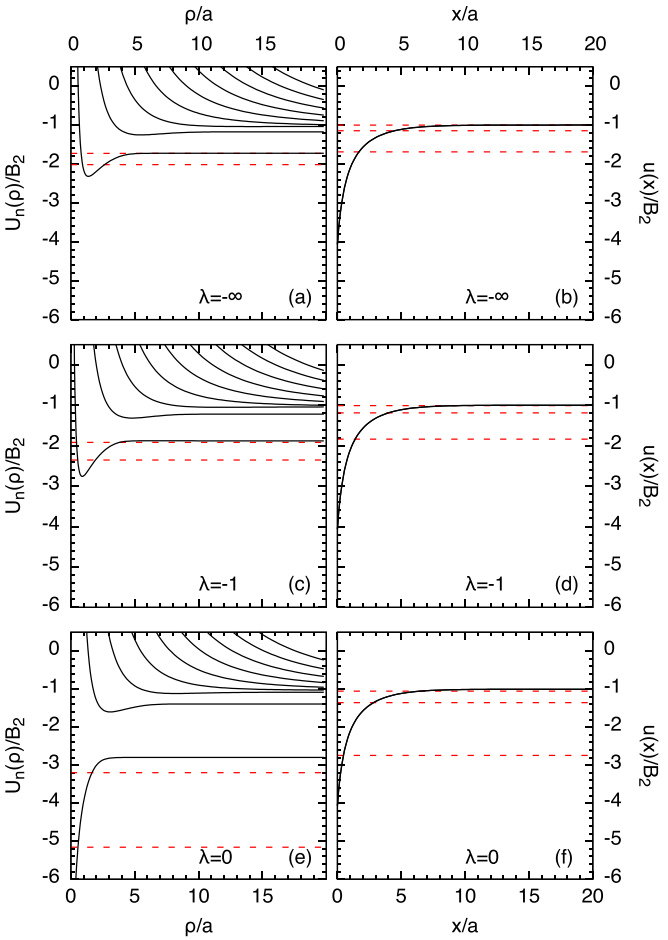

FIG. 1. (Color online) (a), (c), and (e) Hyper-radial potential energy curves $U_n(\rho)$ determined by solving Eq. (11) for $\lambda\to-\infty$, $\lambda=-1$, and $\lambda=0$, respectively. (b), (d) and (f) The corresponding potentials $u(x)$ of Eq. (4). The dashed red lines indicate the energies of tetramer and trimer bound states. All calculations are for $\beta^{-1/2}=4.7$.

Numerical solutions to Eqs. (6), (11), and (13) are found by expressing the desired wave functions as a sum over b splines and solving the resulting generalized eigenvalue problem. We extract $a_{\rm AD}$ and $a_{\rm AT}$ by matching the solutions $\psi(x)$ and $f_0(\rho)$ to a phase-shifted cosine in the asymptotic region. In the case $a_{\rm AD}$, for example, we choose a sufficiently large $x_{\rm max}$ at which we match the log-derivative of the numerically determined eigenfunction of (6) to that of the known asymptotic (large x) form

$$\psi(x)\to\cos(kx)-\tan\delta\sin(kx), \tag{14}$$

thus extracting the phase shift δ. The atom-dimer scattering length is then

$$\frac{1}{a_{\rm AD}}=\lim_{k_{\rm AD}\to0}k_{\rm AD}\tan\delta. \tag{15}$$

It is important to note that we distinguish $k = \sqrt{2\mu_3 E_{\rm rel}}$ from $k_{\rm AD} = \sqrt{2\mu_{23,1} E_{\rm rel}}$ ($E_{\rm rel}$ is the relative collision energy) in the expressions above. The above equations can be applied to extract $a_{\rm AT}$ with the replacements $x \to \rho$, $\psi \to f_0$, $k_{\rm AD} \to k_{\rm AT} = \sqrt{2\mu_{234,1} E_{\rm rel}}$, and with the boundary condition $f_0(0) = 0$. In practice, the limit in Eq. (15) is calculated as the zero energy intercept of a linear fit to $k_{\rm AD} \tan\delta$ at low energy.

A. Scattering lengths $a_{\rm AD}$ and $a_{\rm AT}$

In Fig. 2 we show contour plots of the atom-dimer scattering length $a_{\rm AD}$ and the atom-trimer scattering length $a_{\rm AT}$ on the plane formed by $\tan^{-1}(-\lambda)$ and $\beta^{-1/2}$. We consider only the lowest atom-trimer channel for the elastic collision $H + HHL \to H + HHL$ when calculating $a_{\rm AT}$. All higher scattering channels are energetically closed for all ρ, and their effect is negligible in comparison to the EAA. The Born-Oppenheimer method requires the light particle to be bound such that the lowest atom-dimer scattering channel asymptotically contains an HL dimer, describing the elastic collision $H + HL \to H + HL$. Our calculation fails below the dotted line in Figs. 2(a) and 2(b), which is described by the formula $\lambda = \sqrt{2\beta/(1+\beta)}$. Below this line, the lowest atom-dimer scattering threshold contains an HH dimer and a free L atom, and the structure of the three-body phase diagram is fundamentally different [29].

The dashed lines in Figs. 2(a) and 2(b) indicate $a_{\rm AD} \to 0$ and $a_{\rm AT} \to 0$, respectively, while the solid lines indicate $|a_{\rm AD}| \to \infty$ and $|a_{\rm AT}| \to \infty$. All points along the dashed lines are characterized by reflective elastic collisions in the threshold limit. Points along the solid lines are characterized by reflectionless collisions and the appearance of a new bound state. The number of trimer or tetramer bound states is indicated by n in each figure. The present calculation smoothly connects the poles and zeros found along $\lambda = 0$ and $|\lambda| \to \infty$ in [30].

We see from Fig. 2 that the atom-dimer scattering length is typically much larger than the HL scattering length: $a_{\rm AD} \gg a$, while the same is not true of $a_{\rm AT}$. We trace the reason for this back to the behavior of the potential curves in Fig. 1. First, the trimer (ground-state) binding is deeper than the HL binding, and therefore the size of the trimer is correspondingly smaller because it is confined to the deeper portion of the potential $u(x)$. This means that the effective atom-trimer interaction is of shorter range than the atom-dimer interaction, and typically $a_{\rm AD}$ is also large in comparison to $a_{\rm AT}$.

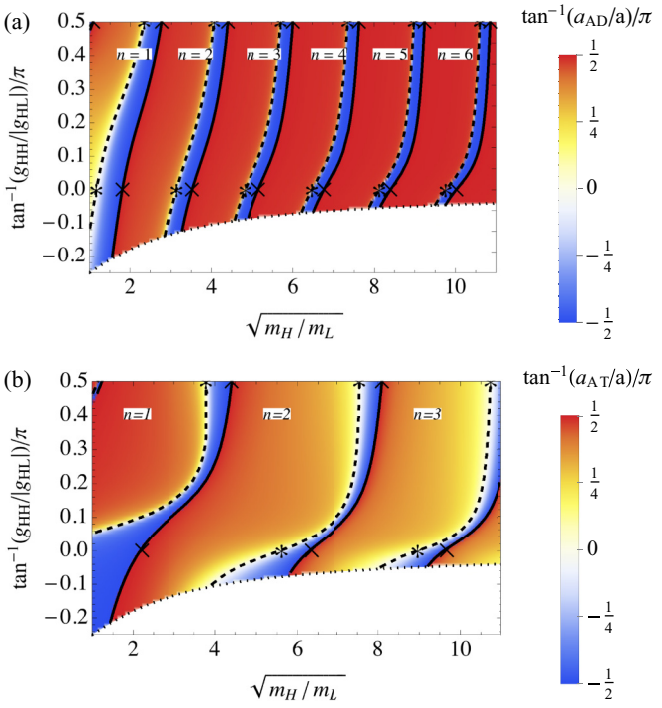

FIG. 2. (Color online) (a) and (b) Contour plots of $a_{\rm AD}$ and $a_{\rm AT}$, respectively, on the plane formed by $\tan^{-1}(g_{\rm HH}/|g_{\rm HL}|)$ and $\sqrt{m_{\rm H}/m_{\rm L}}$. The dashed lines mark the locus of points where the corresponding scattering length vanishes, while the solid lines indicate where it diverges. Along the dotted line, the (HH) binding energy is equal to the (HL) binding.

B. Energy thresholds for few-body processes

In Fig. 3 we show the three-body ground state energy E_3 (blue dotted line) and the four-body ground-state energy E_4 (red dashed line), both calculated in the EAA as a function of $\tan^{-1}(-\lambda)/\pi$ for the Li-Cs mass ratio $\beta^{-1/2} = 4.7$. As one might expect, the energies increase monotonically with increasing $g_{\rm HH}$ due to the increasing H-H repulsion. We also show the bound state energy $2E_2$ for two dimers ($HL + HL$, black line), $E_2 + E_3$ for a dimer plus trimer ($HL + HHL$, black dot-dashed line), $E_2 + E_4$ for a dimer plus tetramer ($HL + HHHL$, purple dot-dot-dashed line), and $2E_3$ for two trimers ($HHL + HHL$, orange long-dash line). Note that for this particular mass ratio, when $\tan^{-1}(-\lambda) < 0.14\pi$, one finds $E_3 < 2E_2$, while for $\tan^{-1}(-\lambda) > 0.14\pi$, $E_3 > 2E_2$. The critical value $\tan^{-1}(-\lambda) = 0.14\pi$ (marked by a black circle) indicates the transition point such that in a gas of dimers, trimer production through the process $HL + HL \to HHL + L$ is energetically allowed for weaker H-H repulsion. Placing the critical value on the plane $\{\beta^{-1/2}, \tan^{-1}(-\lambda)/\pi\} = \{4.7, 0.14\}$ (see Fig. 4) and repeating the calculation for other mass ratios allows the parameter space to be partitioned into regions

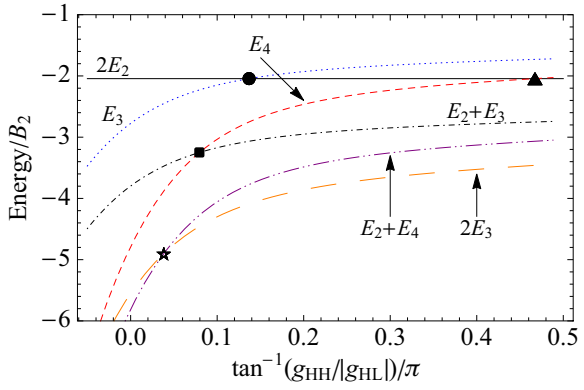

FIG. 3. (Color online) The λ dependence of various energies involving HL, HHL, and $HHHL$ clusters for $\beta^{-1/2} = 4.7$, corresponding to the Li-Cs mass ratio. All energies shown are calculated in the EAA.

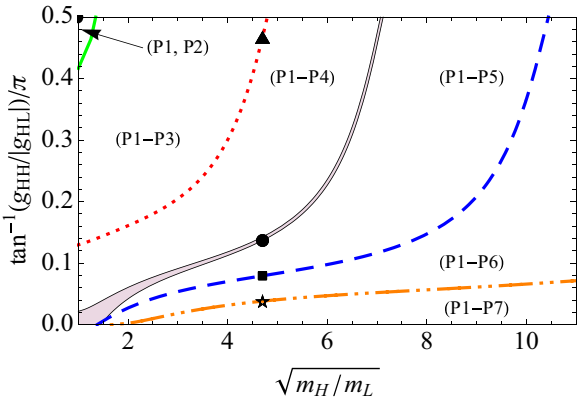

FIG. 4. (Color online) The two-dimensional parameter space is partitioned by lines corresponding to the degeneracy of scattering thresholds. Those processes from Table II that are energetically allowed are listed in each region.

where this process [(P5) in Table II] is either allowed or disallowed. We are able to estimate the error incurred by the Born-Oppenheimer approximation by numerically calculating the line $E_3 = 2E_2$ both in the EAA and the UAA, drawn as the bottom and top black lines, respectively, bounding the shaded band in Fig. 4. We find that the critical mass ratio in the $|\lambda| \to \infty$ limit is $\beta^{-1/2} \approx 7.05$ in the UAA and $\beta^{-1/2} \approx 7.11$ in the EAA, bracketing the previously quoted value $\beta^{-1/2} = 7.0593$ [29].

One can imagine other inelastic processes (listed in Table II) involving three, four, five, and even six particles that have thresholds determined purely by the HL, HHL, and $HHHL$ binding energies. For instance, the rearrangement process (P6) becomes energetically allowed when $E_4 \leqslant E_3 + E_2$. For the specific mass ratio $\beta^{-1/2} = 4.7$, $E_4 = E_3 + E_2$ at $\tan(-\lambda) = 0.08\pi$ as indicated by the black square in Fig. 3. For arbitrary values of $\beta^{-1/2} > 1$, process (P6) becomes energetically allowed below the dashed blue curve in Fig. 4. The three-body recombination processes (P1), (P2), and (P3) are nearly always energetically allowed for $\beta^{-1/2} \geqslant 1$ because there is always an available dimer, trimer, and tetramer state. The only exception is a small region near the Tonks-Girardeau limit ($|\lambda| \to \infty$) where the first trimer state appears exactly at $\beta^{-1/2} = 1$ [29] (the Born-Oppenheimer approximation gives $\beta^{-1/2} \approx 1.08$ [30]), and the first tetramer state does not appear until $\beta^{-1/2} \gtrsim 1.4$ [30]. Therefore, there is a small region in the top left corner of Fig. 4 (bounded by the solid green line) where process (P3) is not allowed because no tetramer state exists. The collision of two trimers may produce a tetramer and a dimer through process (P7) only for values of g_{HH} to the left of the star in Fig. 3 and below the orange dot-dot-dash line in Fig. 4. For the range of mass ratios considered here, (P7) is not allowed for fermionic H atoms. Inelastic processes such as these can lead to atom loss and thermal heating of the trapped gas. Conversely, atom loss rates can be measured as a signature of such processes.

TABLE II. Various inelastic processes that are energetically allowed in the regions shown in Fig. 4 are listed here.

Inelastic process	Threshold law: $\lvert S_{\rm fi}\rvert^2 \propto E_{\rm col}^{\kappa_{\rm min}}$
(P1) $H+H+L \to HL+H$	$\kappa_{\rm min} = \pi/\lvert\tilde{\phi} - \pi/2\rvert$, $\tan\tilde{\phi} = \sqrt{\beta/(2+\beta)}$
(P2) $HL+H+H \to HHL+H$	$\kappa_{\rm min} = \pi/(2\lvert\tilde{\phi}\rvert)$, $\tan\tilde{\phi} = \sqrt{(1+\beta)/(3+\beta)}$
(P3) $HHL+H+H \to HHHL+H$	$\kappa_{\rm min} = \pi/(2\lvert\tilde{\phi}\rvert)$, $\tan\tilde{\phi} = \sqrt{(2+\beta)/(4+\beta)}$
(P4) $HL+HL+H \to HHHL+L$	$\kappa_{\rm min} = \pi/\lvert\tilde{\phi} - \pi/2\rvert$, $\tan\tilde{\phi} = 1/\sqrt{3+2\beta}$
(P5) $HL+HL \to HHL+L$	$\kappa_{\rm min} = 0$
(P6) $HHL+HL \to HHHL+L$	$\kappa_{\rm min} = 0$
(P7) $HHL+HHL \to HHHL+HL$	$\kappa_{\rm min} = 0$

We have labeled each region in Fig. 4 by the set of reactions listed in Table II that are energetically allowed in the forward direction. At sufficiently low temperatures, the energy dependence of the reaction rates for these processes is governed by the corresponding Wigner threshold law. For each of the three-body recombination processes (P1–P4), the threshold law gives $|S_{\rm fi}|^2 \propto E_{\rm col}^{\kappa_{\rm min}}$, where $\kappa_{\rm min}$ is the hyperangular quantum number for the lowest three-body hyperspherical harmonic in the limit of large hyper-radius $R \to \infty$ [35]. In general, $\kappa_{\rm min}$ is an irrational number determined purely by the masses of the collision partners. We list the corresponding values of $\kappa_{\rm min}$ in Table II. The energy dependence of scattering probabilities of two-body processes (P5–P7) is controlled not by the momentum in the entrance channel, but rather in the fragmentation channel [36,37]: $|S_{\rm fi}|^2 \propto k_f$, and therefore approaches a constant at threshold if the fragmentation channel lies below the entrance channel. With the exception of (P3), each of the processes in Table II becomes allowed in the reverse direction on the opposite side of the corresponding critical line in Fig. 4.

IV. CONCLUSION

We have calculated atom-dimer and atom-trimer scattering lengths, as well as trimer and tetramer energies for the homogeneous 1D HHL and $HHHL$ systems as a function of the mass ratio $\beta = m_{\rm L}/m_{\rm H}$ and coupling ratio $\lambda = g_{\rm HH}/g_{\rm HL}$. We expect our purely 1D calculation to be relevant to current experiments with atomic mixtures in 2D optical lattices in the "BCS" limit, when $a_\perp/a_{3\rm D} \to -\infty$ such that the 1D dimer is weakly bound and has large axial extent compared to $a_\perp$. When the few-body system contains only one L impurity, or one ignores the L-L interaction, all eigenstates are parametrized by the ratios $\lambda = g_{\rm HH}/g_{\rm HL}$ and $\beta = m_{\rm L}/m_{\rm H}$. We have determined the regions in this parameter space where certain inelastic processes involving HL, HHL, and $HHHL$ clusters are energetically allowed, potentially leading to atom loss or heating.

Finally, we note that the potential curves shown in Fig. 1 can be used to calculate the energy-dependent scattering cross section for the three-body recombination process $H + H + HL + H + HHL$. Such calculations are beyond the scope of this paper, but may be pursued in the future.

ACKNOWLEDGMENTS

N.P.M. would like to thank D. Blume and J. P. D'Incao for insightful discussions, and A. G. Volosniev for comments on

the manuscript. N.P.M. also thanks the Institute for Nuclear Theory at the University of Washington for its hospitality and the Department of Energy for partial support during the completion of this work.

[1] M. A. Cazalilla, R. Citro, T. Giamarchi, E. Orignac, and M. Rigol, Rev. Mod. Phys. **83**, 1405 (2011).
[2] X.-W. Guan, M. T. Batchelor, and C. Lee, Rev. Mod. Phys. **85**, 1633 (2013).
[3] B. Paredes, A. Widera, V. Murg, O. Mandel, S. Fölling, I. Cirac, G. V. Shlyapnikov, T. W. Hänsch, and I. Bloch, Nature (London) **429**, 277 (2004).
[4] H. Moritz, T. Stöferle, M. Köhl, and T. Esslinger, Phys. Rev. Lett. **91**, 250402 (2003).
[5] T. Kinoshita, T. Wenger, and D. S. Weiss, Nature (London) **440**, 900 (2006).
[6] E. Lieb and W. Liniger, Phys. Rev. **130**, 1605 (1963).
[7] E. H. Lieb, Phys. Rev. **130**, 1616 (1963).
[8] J. B. McGuire, J. Math. Phys. **5**, 622 (1964).
[9] M. Olshanii, Phys. Rev. Lett. **81**, 938 (1998).
[10] T. Bergeman, M. G. Moore, and M. Olshanii, Phys. Rev. Lett. **91**, 163201 (2003).
[11] I. S. Gradshteyn and I. M. Ryzhik, in *Table of Integrals, Series and Products*, 7th ed., edited by A. Jeffrey and D. Zwillinger (Academic, New York, 2014).
[12] G. E. Astrakharchik, D. Blume, S. Giorgini, and B. E. Granger, Phys. Rev. Lett. **92**, 030402 (2004).
[13] G. E. Astrakharchik, D. Blume, S. Giorgini, and B. E. Granger, J. Phys. B **37**, S205 (2004).
[14] H. Moritz, T. Stöferle, K. Günter, M. Köhl, and T. Esslinger, Phys. Rev. Lett. **94**, 210401 (2005).
[15] C. Mora, R. Egger, and A. O. Gogolin, Phys. Rev. A **71**, 052705 (2005).
[16] C. Mora, A. Komnik, R. Egger, and A. O. Gogolin, Phys. Rev. Lett. **95**, 080403 (2005).
[17] A. Wenz, G. Zürn, S. Murmann, I. Brouzos, T. Lompe, and S. Jochim, Science **342**, 457 (2013).
[18] J. Catani, G. Lamporesi, D. Naik, M. Gring, M. Inguscio, F. Minardi, A. Kantian, and T. Giamarchi, Phys. Rev. A **85**, 023623 (2012).
[19] G. Pagano, M. Mancini, G. Cappellini, P. Lombardi, F. Schäfer, H. Hu, X.-J. Liu, J. Catani, C. Sias, M. Inguscio, I. Massimo, and L. Fallani, Nat. Phys. **10**, 198 (2014).
[20] S. E. Gharashi and D. Blume, Phys. Rev. Lett. **111**, 045302 (2013).
[21] S. E. Gharashi, K. M. Daily, and D. Blume, Phys. Rev. A **86**, 042702 (2012).
[22] T. Sowiński, T. Grass, O. Dutta, and M. Lewenstein, Phys. Rev. A **88**, 033607 (2013).
[23] S. E. Gharashi, X. Y. Yin, Y. Yan, and D. Blume, Phys. Rev. A **91**, 013620 (2015).
[24] E. Lindgren, J. Rotureau, C. Forssén, A. Volosniev, and N. T. Zinner, New J. Phys. **16**, 063003 (2014).
[25] A. Volosniev, D. V. Fedorov, A. S. Jensen, M. Valiente, and N. T. Zinner, Nat. Commun. **5**, 5300 (2014).
[26] J. Levinsen, P. Massignan, G. M. Bruun, and M. M. Parish, Sci. Adv. **1**, e1500197 (2015).
[27] A. S. Dehkharghani, A. G. Volosniev, and N. T. Zinner, Phys. Rev. A **92**, 031601(R) (2015).
[28] M. D. Girardeau, J. Math. Phys. **1**, 516 (1960).
[29] O. I. Kartavtsev, A. V. Malykh, and S. A. Sofianos, Zh. Eksp. Teor. Fiz. **135**, 419 (2009) [JETP **108**, 365 (2009)].
[30] N. P. Mehta, Phys. Rev. A **89**, 052706 (2014).
[31] V. F. Brattsev, Sov. Phys. Dokl. **10**, 44 (1965).
[32] S. T. Epstein, J. Chem. Phys. **44**, 836 (1966).
[33] A. F. Starace and G. L. Webster, Phys. Rev. A **19**, 1629 (1979).
[34] H. T. Coelho and J. E. Hornos, Phys. Rev. A **43**, 6379 (1991).
[35] N. P. Mehta, B. D. Esry, and C. H. Greene, Phys. Rev. A **76**, 022711 (2007).
[36] C. W. Clark, Phys. Rev. A **28**, 83 (1983).
[37] H. R. Sadeghpour, J. L. Bohn, M. J. Cavagnero, B. D. Esry, I. I. Fabrikant, J. H. Macek, and A. R. P. Rau, J. Phys. B **33**, R93 (2000).